Available online at www.sciencedirect.com
SCIENCE DIRECT®
International Journal of Solids and Structures 42 (2005) 2211–2224
INTERNATIONAL JOURNAL OF SOLIDS and STRUCTURES
www.elsevier.com/locate/ijsolstr

Symmetric and asymmetric deformation transition in the regularly cell-structured materials. Part II: Theoretical study

Kanyatip Tantikom [a,*], Tatsuhiko Aizawa [b,*], Toshiji Mukai [c]

[a] *Graduate School of Engineering, The University of Tokyo, Tokyo 153-8904, Japan*
[b] *Center for Collaborative Research, The University of Tokyo, Tokyo 153-8904, Japan*
[c] *National Institute for Materials Science, Tsukuba, Ibaraki 305-0047, Japan*

Received 4 June 2004; received in revised form 18 September 2004
Available online 28 October 2004

Abstract

Symmetric and asymmetric deformation behavior is theoretically analyzed for regularly cell-structured materials. On the basis of the elasto-plastic formulation by the finite element method, the computational model is constructed in order to understand the effect of various parameters on the deformation mode transition. Symmetric deformation changes itself to asymmetric deformation when increasing the nominal compressive strain. Effects of the relative density, the contact length, and the adhesive bonding on this mode transition are investigated under quasi-static in-plane compression. Besides the relative density, the contact length to thickness ratio (r_c/t) plays an important role on the symmetric–asymmetric deformation transition. The intercell stress transfer also has an influence on the stability of the cell-structure during crushing. The theoretical prediction is compared with the experimental results in (Part 1) to quantitatively discuss the compressive deformation of regularly cell-structured materials.

Keywords: Cell-structured materials; Finite element analysis; Collapsing deformation; Deformation mode transition; Local stress transfer

* Corresponding authors. Address: Department of Metallurgy, The University of Tokyo, Meguro ku Komaba, Tokyo 1530041, Japan. Tel.: +81 906 184 8349; fax: +81354 525 116 (K. Tantikom), tel.: +84 3 5452 5086; fax: +84 3 5452 5116 (T. Aizawa).
E-mail addresses: kanyatip@odin.hpm.rcast.u-tokyo.ac.jp (K. Tantikom), aizawa@odin.hpm.rcast.u-tokyo.ac.jp (T. Aizawa).

0020-7683/$ - see front matter
doi:10.1016/j.ijsolstr.2004.09.027

1. Introduction

Two-dimensional cellular structures have been widely used as models to study the mechanical properties of cellular materials. (Gibson and Ashby, 1988; Papka and Kyriakides, 1998a; Guo and Gibson, 1999; Chung and Waas, 2002a,b). Ashby and Gibson presented various theoretical and empirical expressions to describe their mechanical properties. The moduli and collapse strengths of cellular solids are defined as a function of the relative density. They also proposed the mechanism for compressive deformation of honeycombs and foams, and showed how the stress–strain curve changes with increasing the relative density or the fraction of thickness to cell wall length (t/l). Many researchers (Fortes and Ashby, 1999; Albuquerque et al., 1999; Chen et al., 2001) tried to predict the degradation in mechanical responses of cellular structures, containing geometric imperfections and/or irregularity of cell-alignment by theoretical analysis. Simone and Gibson (1998) used the finite element method to examine the effect of the cell wall thickness varying along the length of the cell edge and the effect of curvature and corrugations in honeycombs. Variation of the cell wall thickness along the length of cell edge, affects the elastic modulus and plastic collapsing stress of honeycombs. The structural defects by missing or broken walls in the cell-structured materials leads to large reduction in the elastic modulus and strength in both regular and irregular structures (Albuquerque et al., 1999). Silva and Gibson (1997) found that elimination of cell walls by 5% results in reduction of modulus and strength for honeycomb over 35%. A little morphological imperfection and/or inhomogeneity in cell-structure can initiate the local deformation of the cell-structured materials.

Papka and Kyriakides (1994, 1998a,b), Chung and Waas (2002a,b) pointed out that the compressive response of regularly aligned honeycomb is very sensitive to the induced instability by the shear-type deformation. This shear deformation commences as a localized deformation in the narrow zone and is followed by subsequent collapsing of cells throughout the specimen until each cell wall is in contact and every material wall is compressed. This deformation mechanism reflects on the stress–strain curve. After elastic response, the onset of shear localization corresponds to the initial yielding in the stress–strain curve, and, the successive cell-collapsing, to the stress plateau region with nearly constant stress until the onset of densification stage.

Tantikom et al. (2004) first stressed that the regularly cell-structured materials undergoes uniform, symmetric deformation in compression under the optimum geometric configuration. Through the experimental studies (Tantikom et al., in press, part 1), symmetric deformation changes itself to asymmetric deformation mode with increasing nominal compressive strain in the case of large contact length to thickness ratio. In the present study, a theoretical model is constructed by using the finite element analysis to describe the in-plane compressive behavior for regularly cell-structured materials. Through the parameter sensitivity analysis, the effect of the relative density, the contact length and the intercell adhesive bonding on the compressive deformation is discussed to investigate the deformation mode transition. Furthermore, the experimental results in (part 1) are directly verified by this theoretical modeling for the measured stress–strain curve and sequence of deformed geometric configuration.

2. Theoretical modeling

The finite element analysis was employed as a theoretical model to describe the in-plane compressive deformation mechanism of the cell-structured materials. The related computational conditions are summarized in Table 1. The copper cell-structured assembly was assumed to be perfect in geometry with the radius of R and the wall thickness of t. The thickness was varied to control the relative density. The contact condition in joining was also varied to understand the stress transfer through the cell-structured materials. Each cell wall was subdivided into the finite elements. Typical mesh subdivision is illustrated in Fig. 1.

Table 1
Computational conditions

Program system	ANSYS6.1
Type of element	Triangular element (6 nodes)
Young's modulus	$E = 100\,\text{GPa}$
Poisson's ratio	$v = 0.35$
Stress-strain curve	Bilinear isotropic hardening (rate-independent plasticity)
Plastic modulus	$K = 1\,\text{GPa}$
Friction coefficient	0.3
Yielding condition	J_2 flow theory

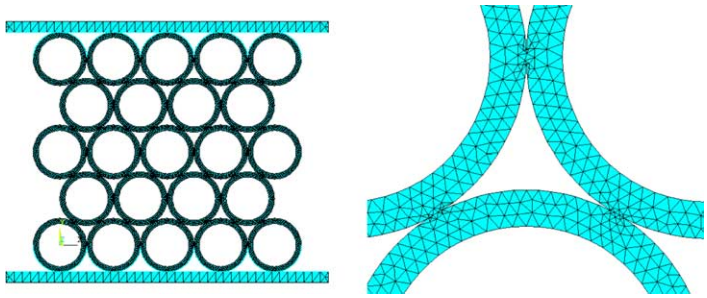

Fig. 1. Mesh subdivision of cell walls and their contact region in the finite element model.

The following simulation was conducted by the two-dimensional quasi-static analysis. The contact and target elements were used to trace the change of contact state in deforming cell-tubes. The target-element was utilized to predict the possibility of penetration of one cell-element to the others. The contact-element was necessary to characterize the stress–strain state between deforming elements in contact. The cell-wall material was assumed to be elasto-plastic with the J_2-flow theory. Its stress–strain relationship was represented by the bilinear isotropic hardening model. The elastic contribution was characterized by the Young's modulus (E) while the elasto-plastic response was modeled by the plastic modulus (K). Considering that experimental specimen is uniaxially compressed by upper and lower rigid bars, two bars were modeled by the rigid surface. The lower rigid surface was fixed and the upper one was controlled to press the finite element model with the prescribed incremental displacement. Temporal evolution of geometric configuration was obtained in series by this displacement control.

Finite element analysis was conducted to consider the effect of number of rows on the stress–strain responses. In general, the loading condition overwhelms the intrinsic stress–strain response when the number of rows is small. Hence, the adequate number of rows is necessary to obtain the stress–strain relation, which is indifferent to the number of rows. Fig. 2 compares the nominal stress–strain relations among three-row, five-row and seven-row aligned assemblies. These assemblies have the same radius, thickness and contact length of 500 μm, 100 μm and 21 μm, respectively. All of the cell-structured assemblies have positive strain hardening with $\mathrm{d}\sigma_c/\mathrm{d}\varepsilon_c > 0$ in the initial collapsing stage. When using the three-row assembly, the elastic deformation of cell-structured material is never simulated. In similar manner to the experimental results, the linear elastic region is reproduced in the calculated stress–strain relations by using the five-row and seven-row models. These dissimilar features are caused by the different number of cells, which are adjacent to the punches. The deformation of adjacent cells to the punches is constrained by loading motion of the upper and lower punches, so that the top and bottom end rows have higher stiffness than other inner cells. Agreement of stress–strain response between five and seven-row models assures that the regularly

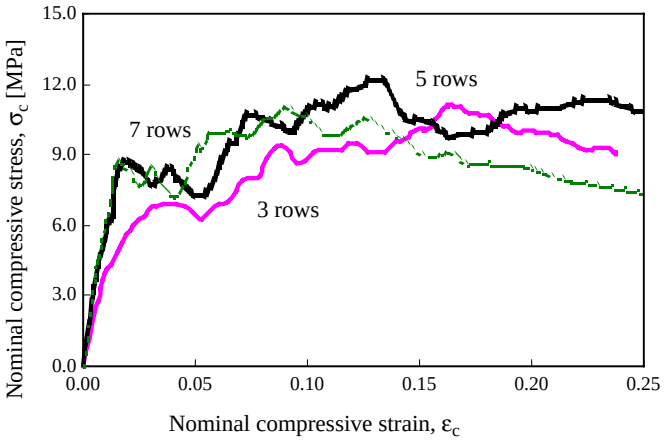

Fig. 2. In-plane compressive stress–strain curves of cell-structured models with different number of rows.

assembled model has intrinsic stress–strain relationship when the number of rows is larger or equal to five rows. In the following studies, five-row assembly is employed as a common geometric configuration for standard cell-structured materials.

3. Verification of experimental results

In part 1, it was experimentally described that the regularly cell-structured materials collapse both in the symmetric and asymmetric modes. A perfect circular cell-structured assembly with five-row and five-column, close-packed hexagonal array, is used as a theoretical model in order to verify those experimental results. As listed in Table 2, two cases are considered. Among the geometric parameters, the radius and thickness of cells as well as the relative density are constant. Only the contact length, r_c is different between two.

3.1. Symmetric-mode deformation

Fig. 3 depicts the sequence of deformed geometry with increasing the nominal strain, ε_c in the Case-1. The regularly cell-structured material deforms symmetrically, keeping the original hexagonal array unchanged. Each cell in the assembly except for the top and bottom ends uniformly deforms during uniaxial compression. A cell located at the center of assembly is employed as a representative cell to calculate the local strain. As shown in Fig. 4, the calculated logarithmic local strain (ε^*) is proportional to the nominal strain. Little or no spin rotation is accompanied with this compressive deformation. Namely, the cell-structured assembly is uniformly strained during compression to preserve the initial topological configuration.

Table 2
Finite element model configurations of regularly cell-structured models

Model	Radius of cell, R (μm)	Cell wall thickness, t (μm)	Relative density, ρ_R	Contact length, r_c (μm)	r_c/t
Case-1	500	100	0.29	18	0.18
Case-2	500	100	0.29	32	0.32

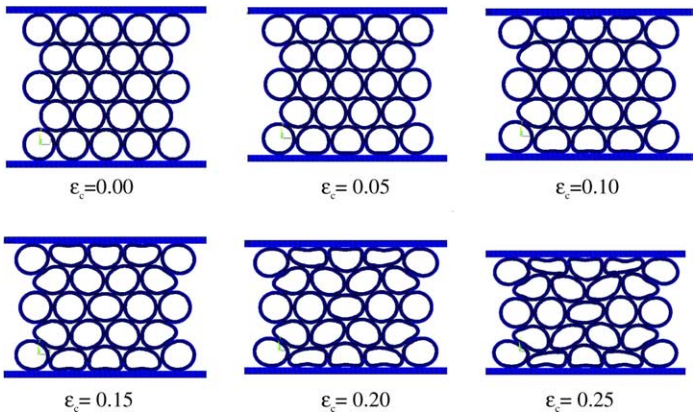

Fig. 3. Sequence of symmetrically deformed cell-structured assembly.

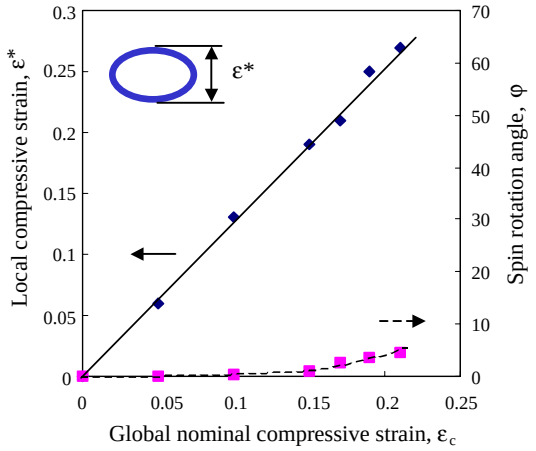

Fig. 4. Compressive straining of representative cell-structured material.

Fig. 5 compares the experimentally measured and theoretically calculated stress–strain relations. The solid line denotes the stress–strain curve by the finite element analysis, and the dotted line, the experimental result. In computation, the initial elastic responses as well as the reduction of stiffness and stress in the initial yielding are distinctly observed as a common behavior to metallic cell-structured materials (Shim and Stronge, 1986; Papka and Kyriakides, 1998a,b). Both stress–strain relations are in good agreement until the onset of densification stage. To be noted here in both results, the work hardening takes place in the collapsing region. This assures that positive stress increment is necessary to have the cell-structured assembly deform in symmetric and uniform. Fig. 6 also compares the deformed geometric configuration of assemblies in both results.

3.2. Asymmetric-mode deformation

Fig. 7 depicts the sequence of deformed geometry with increasing the nominal strain, ε_c in the Case-2. The regularly cell-structured material deforms asymmetrically with a shear-type localization in a narrow

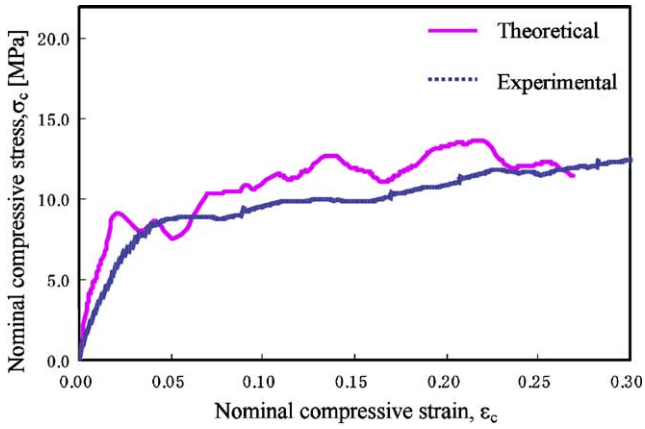

Fig. 5. Comparison between experimental and finite element results in the symmetric deformation.

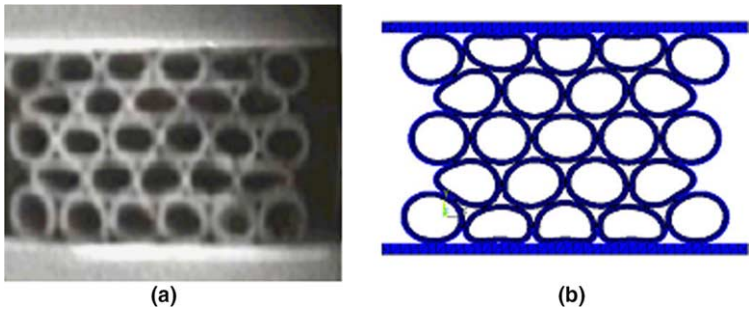

Fig. 6. Comparison of deformed assemblies between (a) experimental result and (b) finite element analysis at $\varepsilon_c = 0.18$.

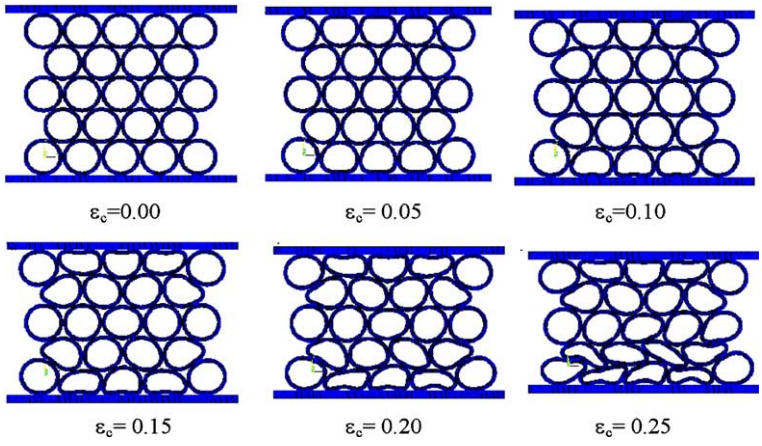

Fig. 7. Sequence of asymmetrically deformed cell-structured assembly.

zone. In this case, cells in the second row from the bottom begin to make shear-deformation while the remote cells from this zone, near the top of specimen, remain to be in symmetric deformation. This local

collapsing deformation progresses successively in each two neighboring row until it is arrested when the cell walls come into contact.

A cell located at the center of cell-structured array is also employed as a representative cell to calculate the local strain. As shown in Fig. 8, the calculated logarithmic local strain (ε^*) increases abruptly when $\varepsilon_c > 0.15$. Since this cell element locally collapses, it has little loading capacity and plastically deforms in the unconstrained flow when $\varepsilon_c > 0.15$. The local collapsing behavior is accompanied with the significantly large spin rotation.

Fig. 9 compares the experimentally measured and theoretically calculated stress–strain relations for asymmetric deformation. The theoretical response is in agreement with the experimental result. Nearly constant plateau stress is observed in the collapsing region for both results. This asymmetric deformation is commonly observed for circular cell-structured material (Poirier et al., 1992; Papka and Kyriakides 1998b; Chung and Waas, 2002a,b). Fig. 10 also compares the deformed geometric configuration of assemblies in both results.

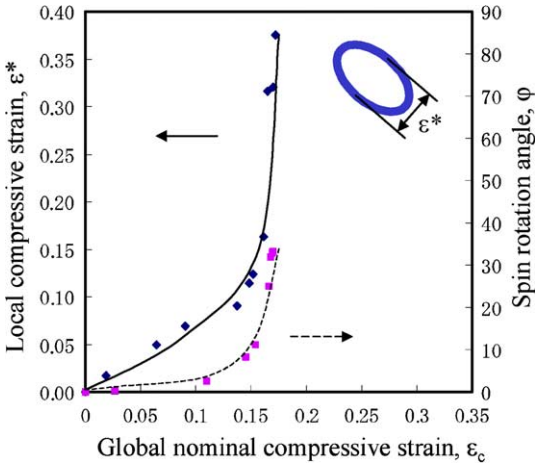

Fig. 8. Compressive straining of regularly cell-structured material.

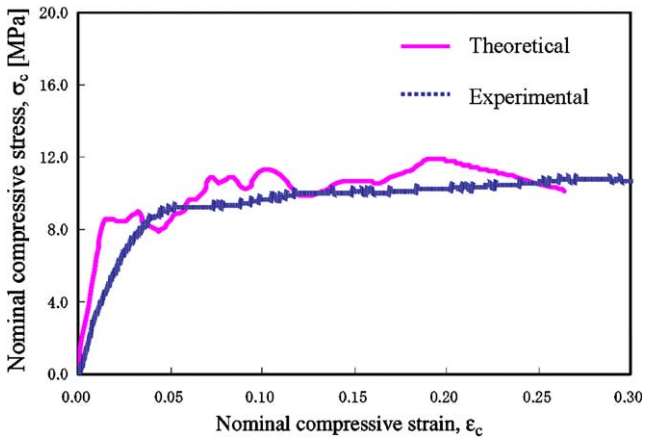

Fig. 9. Comparison between experimental and finite element results in the asymmetric deformation.

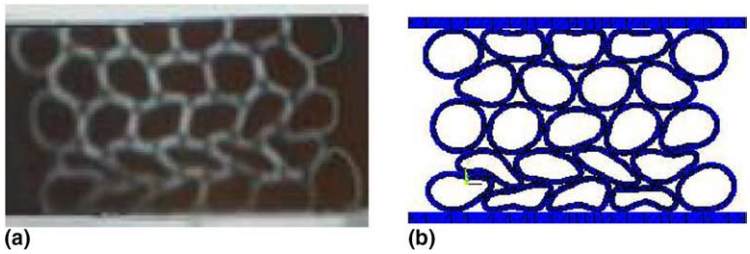

Fig. 10. Comparison of deformed assemblies between (a) experimental result and (b) finite element analysis at $\varepsilon_c = 0.20$.

The experimentally measured stress–strain relation as well as deformed geometry of specimen can be quantitatively simulated by the present theoretical model. Mechanism of symmetric and asymmetric deformation in compression is investigated to understand the effect of various parameters on the difference in the deformation mode.

4. Parameter sensitivity

In the experimental study in part 1 (Tantikom et al., in press), the effect of parameters on the in-plane deformation mechanism of regularly cell-structured material was discussed. The deformation transition from symmetric to asymmetric modes was observed experimentally. In order to verify and complete the mechanical understanding of cell-structured materials, finite element method is employed for theoretical parameter survey to consider the effects of relative density, contact length and also adhesive bonding on this mode transition.

4.1. Relative density

Three cases are considered to study the effect of relative density on the deformation mode transition. As listed in Table 3, the initial, perfect cell-structured assembly has constant cell radius (R) and intercell contact length (r_c). The cell wall thickness (t) is parametrically varied to control the relative density.

Figs. 11 and 12 depict the variation of stress–strain relationships and deformation sequences with increasing the relative density. At the initial stage, all the assemblies commence to collapse in uniform and symmetric. As shown in Fig. 12, however, this symmetric-mode changes itself to asymmetric one when the compressive strain exceeds the critical compressive strain (ε_c^*).

Fig. 13 shows the correlation between critical compressive strain (ε_c^*) and relative density (ρ_R). Monotonic increase of ε_c^* with ρ_R assures that symmetric-mode deformation should be stabilized with increasing the relative density. In fact, when $\rho_R \geqslant 0.3$, the symmetric-mode deformation overwhelms the collapsing stage in the stress–strain relation.

Table 3
Finite element model configurations of regularly cell-structured models

Model	Radius of cell, R (μm)	Cell wall thickness, t (μm)	Relative density, ρ_R	Contactlength, r_c (μm)	r_c/t
Case-1	500	80	0.24	32	0.40
Case-2	500	100	0.29	32	0.32
Case-3	500	120	0.34	32	0.26

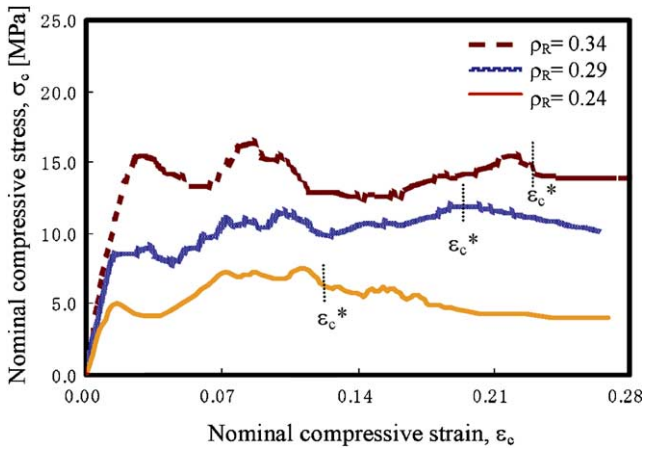

Fig. 11. In plane compressive stress–strain relationships of cell-structured models with different relative densities.

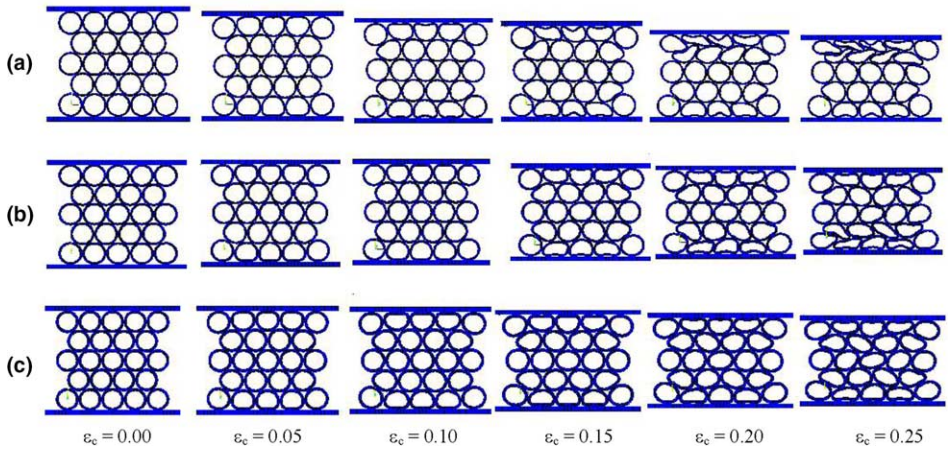

Fig. 12. Deformed sequences of assemblies corresponding to the stress–strain curves in Fig. 11. (a) $\rho_R = 0.24$, (b) $\rho_R = 0.29$, and (c) $\rho_R = 0.34$.

4.2. Contact length

The contact length was varied with $\rho_R = 0.29$ to study the effect of contact length on the deformation mode transition, as listed in Table 4. Fig. 14 depicts in-plane nominal compressive stress–strain relationships for various contact lengths. All of the finite element models experience linear deformation initially. The stress–strain curves in this elastic region are indifferent to each model. The difference in the plastic collapsing stress is caused by the stress transfer and deformation mode of assemblies, as shown in Fig. 15. With increasing the contact length, r_c, the symmetric deformation mode changes itself to the asymmetric shear-deformation mode. In case of the smallest contact length, $r_c = 19$, the assembly deforms in uniform and symmetric. Work-hardening takes place in collapsing region. In the stress–strain curve for $r_c^* = 0.21$, both the yielding and collapsing stresses become the highest. This maximum loading capacity corresponds to the mode change from symmetric to asymmetric deformation. This r_c^* is the optimum contact length with

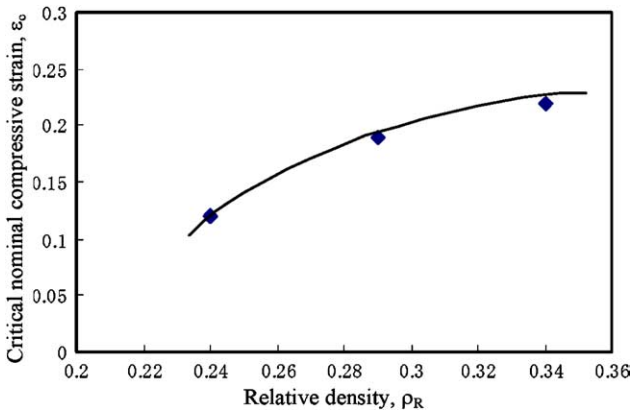

Fig. 13. Relationship between critical nominal compressive strain and relative density of regularly cell-structured materials.

Table 4
Finite element model configurations of regularly cell-structured models

Model	Radius of cell, R (μm)	Cell wall thickness, t (μm)	Relative density, ρ_R	Contact length, r_c (μm)	r_c/t
Case-1	500	100	0.29	19	0.19
Case-2	500	100	0.29	21	0.21
Case-3	500	120	0.29	31	0.31

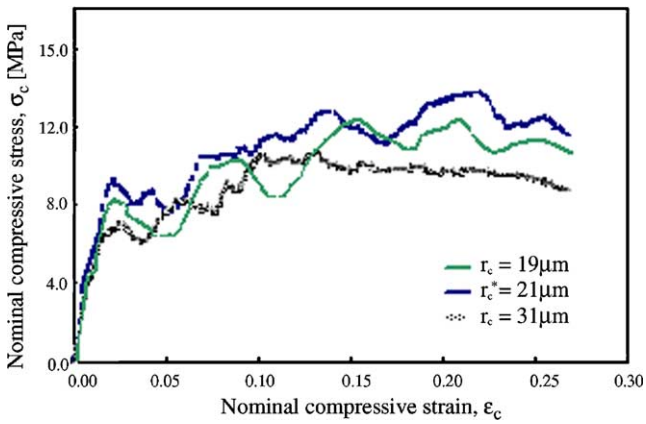

Fig. 14. In plane compressive stress–strain relationships of cell-structured model with different contact lengths.

the highest stress transfer across the contact area. When $r_c > r_c^*$, shear-localization is promoted from the weakest cell and it spreads from one collapsing zone to its neighboring cells, results in the nearly constant stress plateau in collapsing region.

In the symmetric deformation (Fig. 15(a)), the stress transfers in the symmetric parallelogram through the compressive loading. No distortion takes place, preserving the symmetric stress transfer. In the asymmetric deformation (Fig. 15(c)), the stress state localizes among the neighboring cells, forming the polygonal network for local stress transfer. This local geometric change in regularity reflects on the global deformation mode change and the reduction of loading capacity of cell-structured materials.

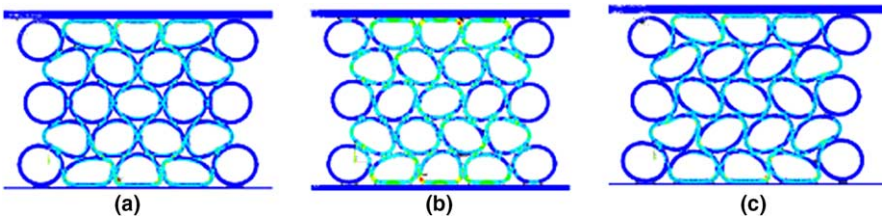

Fig. 15. Stress transfer across the contact area at $\varepsilon_c = 0.15$ for (a) symmetric mode, $r_c = 19\,\mu m$ (b) mixed mode, $r_c = 21\,\mu m$, and (c) asymmetric mode, $r_c = 31\,\mu m$.

In Fig. 15(b), both symmetric and asymmetric modes are mixed to make maximum stress transfer across the contact area with uniform deformation.

Both relative density (ρ_R or t) and contact length have significant effects on the deformation mode transition. For further understanding of these effects, contact length to thickness ratio, r_c/t, is selected as an indicator to describe the deformation mode transition of regularly cell-structured materials.

4.3. Contact length to thickness ratio (r_c/t)

Depending on r_c/t or ρ_R, the symmetric-mode deformation changes itself to the asymmetric one at the critical nominal compressive strain, ε_c^*. When ε_c^* is small, nearly the whole deformation advances in the asymmetric-mode. Increase of ε_c^* promotes stabilization of uniform symmetric deformation. Fig. 16 depicts the correlation between ε_c^* and r_c/t for various relative densities. At the same relative density, the ε_c^* decreases with increasing r_c/t. Namely, asymmetric deformation is preferable to be selected with increasing r_c/t. For $r_c/t > 0.3$, ε_c^* approaches to a constant value, ε_c^{**}, which is indifferent to r_c/t and only dependent on ρ_R. In the lower relative density materials, ε_c^{**} decreases with ρ_R and $\varepsilon_c^* \sim \varepsilon_c^{**}$. Asymmetric-mode is selected in the lower relative density materials irrespective of r_c/t. In the higher relative density, $\varepsilon_c^* > \varepsilon_c^{**}$ for $r_c/t < 0.3$. Symmetric deformation is selected as a more stable equilibrium path. Since ε_c^{**} increases monotonically with ρ_R, asymmetric deformation mode is never selected as an elasto-plastically collapsing deformation in the regularly assembled cell-structured materials.

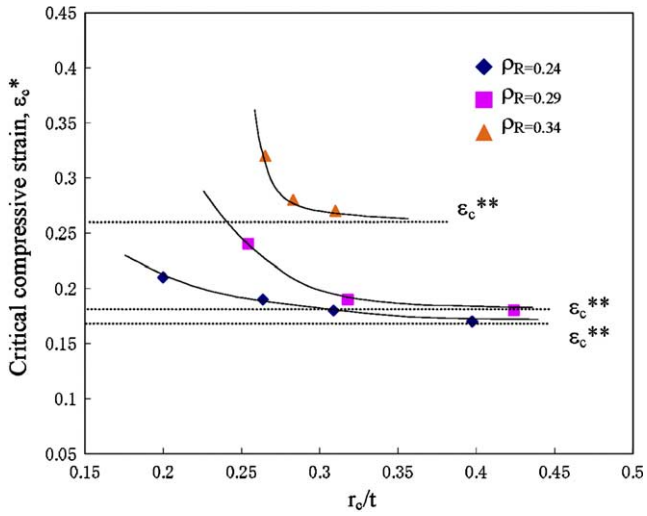

Fig. 16. Sensitivity of critical compressive strain to r_c/t and relative density.

4.4. Adhesive bonding

Regularly cell-structured material with dipped resin was simulated in order to understand the effect of local stress transfer on the deformation mode transition. The initial configuration was assumed to have the radius of 500 μm, the thickness of 100 μm, the contact length of 25 μm with $r_c/t = 0.25$, and the relative density of 0.29. Liquid epoxy resin was located at the triplet corners among the perfect cell walls. The resin was assumed to be elastic and to have the Young's modulus of 8 GPa and the Poisson ratio of 0.49. Fig. 17 compares stress–strain relationships among the experimental result and two finite element results with and without resin. The simulated response is in nearly good agreement with the experimental result. Work-hardening in the collapsing region takes place with increasing ε_c in both simulated and experimental results. The deformed configuration in the finite element model corresponds well to the actual deformed specimen, as shown in Fig. 18.

Fig. 19 depicts the deformed sequences for two models with and without resin. The symmetric to asymmetric-mode transition is observed in the materials without the dipped resin: $\varepsilon_c^* = 0.23$ for $r_c/t = 0.25$. The dipped resin is a deformable buffer to assist to support the compressive load. Since this deformable buffer makes local intercell stress transfer more isotropic, the symmetric collapsing mode is selected as a stable deformation state in compression. Hence, improvement of local stress transfer leads to high loading capacity at high yielding and collapsing stresses.

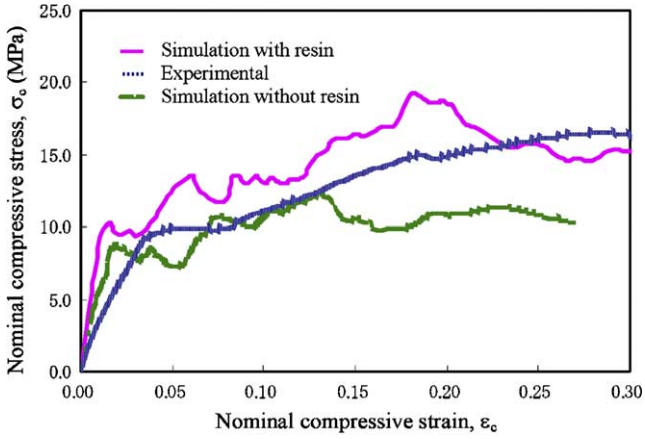

Fig. 17. Comparison between experimental and finite element results in the dipped resin assemblies.

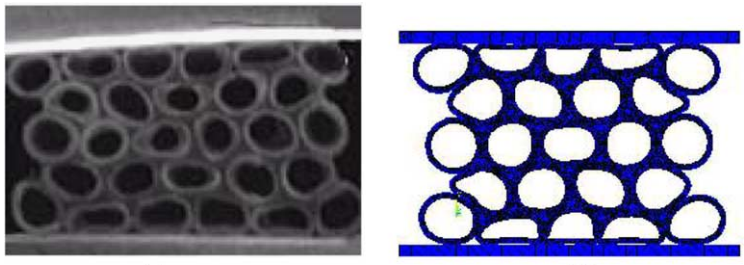

Fig. 18. Comparison of deformed assemblies at $\varepsilon_c = 0.2$ between (a) experimental result and (b) finite element analysis.

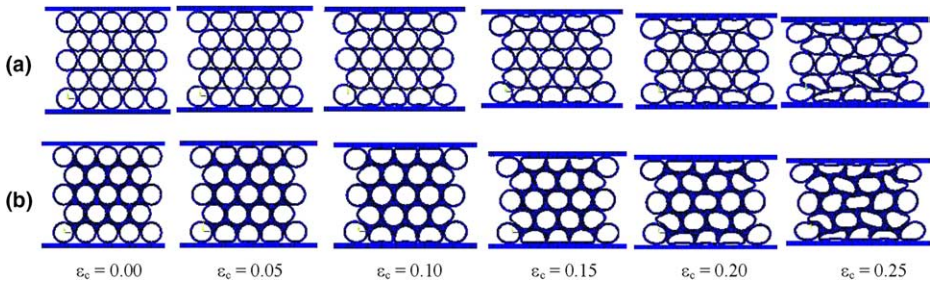

Fig. 19. Deformed sequences of assemblies corresponding to the stress–strain curves in Fig. 17. (a) Ordinary cell-structured model and (b) dipped resin finite element model.

5. Conclusions

In-plane compression of regularly cell-structured materials has been simulated theoretically through the finite element analysis. In order to complete the understanding of the relative density, the contact length and the adhesive bonding on the deformation transition, various finite element models were employed to simulate the stress–strain relation and temporal evolution of geometries under quasi-static in-plane compression. The experimental results were compared to the theoretical study with quantitatively good agreement. The relative density has a significant effect on the deformation mode transition and the stress–strain response. With the same contact length, symmetric deformation preserves in the higher relative density materials whereas the asymmetric deformation commonly takes place in the low relative density cell-structured assembly. The contact length and/or contact length to thickness ratio (r_c/t) play an important role on this deformation transition and collapsing stress of cell-structured materials. With increasing contact length and/or r_c/t, asymmetric deformation is selected as more preferable stable to symmetric one. In particular, high relative density materials are sensitive to this r_c/t. The deformable buffer material among connected cell walls assists to support the compressive load and to stabilize the symmetric deformation mode.

Acknowledgement

This study is financially supported in part by the grant-in-aid from MEXT for the national project on the barrier-free processing and the environmentally benign manufacturing.

References

Albuquerque, J.M., Vaz, M.F., Fortes, M.A., 1999. Scr. Mater. 41 (2), 167–174.
Chen, C., Lu, T.J., Fleck, N.A., 2001. Int. J. Mech. Sci. 43, 487–504.
Chung, J., Waas, M.A., 2002a. AIAA J. 40 (5), 974–980.
Chung, J., Wass, M.A., 2002b. Int. J. Impact Eng. 27, 729–754.
Fortes, M.A., Ashby, M.F., 1999. Acta Mater. 47, 3469–3473.
Gibson, L.J., Ashby, M.F., 1988. Cellular Solids Structure and Properties. Cambridge University Press, Cambridge, MA.
Guo, X.E., Gibson, J.L., 1999. Int. J. Mech. Sci. 41, 85–105.
Papka, S.D., Kyriakides, S., 1994. J. Mech. Phys. Solids 42, 1499–1532.
Papka, S.D., Kyriakides, S., 1998a. Acta Mater. 46 (8), 2765–2776.
Papka, S.D., Kyriakides, S., 1998b. Int. J. Solids Struct. 35 (3–4), 239–267.
Poirier, C., Ammi, M., Bideau, D., Troadeem, J.P., 1992. Phy. Rev. Lett. 68 (2), 216–219.
Shim, V.P.W., Stronge, W.J., 1986. Int. J. Mech. Sci. 28 (10), 709–728.

Silva, M.J., Gibson, J.L., 1997. Int. J. Mech. Sci. 39, 549–563.
Simone, A.E., Gibson, L.J., 1998. Acta Mater. 46, 3929–3935.
Tantikom, K., Suwa, Y., Aizawa, T., 2004. Mater. Trans. JIM 45 (2), 509–515.
Tantikom, K., Aizawa, T., Mukai, T., Int. J. Solids Struct., in press.